AGU PUBLICATIONS

Geophysical Research Letters

RESEARCH LETTER
10.1002/2016GL069483

Key Points:
- Transdimensional Bayesian ambient noise tomography is performed in northeast Asia
- Low velocities at asthenospheric depths extend away from back arcs to thick continental margins
- The distribution of the intraplate volcanism in the margin correlates with observed low velocities

Supporting Information:
- Supporting Information S1

Correspondence to:
S. Kim,
seongryong.kim@anu.edu.au

Citation:
Kim, S., H. Tkalčić, J. Rhie, and Y. Chen (2016), Intraplate volcanism controlled by back-arc and continental structures in NE Asia inferred from transdimensional Bayesian ambient noise tomography, *Geophys. Res. Lett.*, *43*, 8390–8398, doi:10.1002/2016GL069483.

Received 6 MAY 2016
Accepted 28 JUL 2016
Accepted article online 1 AUG 2016
Published online 16 AUG 2016

Intraplate volcanism controlled by back-arc and continental structures in NE Asia inferred from transdimensional Bayesian ambient noise tomography

Seongryong Kim[1], Hrvoje Tkalčić[1], Junkee Rhie[2], and Youlin Chen[3]

[1]Research School of Earth Sciences, Australian National University, Canberra, ACT, Australia, [2]School of Earth and Environmental Sciences, Seoul National University, Seoul, South Korea, [3]Advanced Technology Division, Array Information Technology, Greenbelt, Maryland, USA

Abstract Intraplate volcanism adjacent to active continental margins is not simply explained by plate tectonics or plume interaction. Recent volcanoes in northeast (NE) Asia, including NE China and the Korean Peninsula, are characterized by heterogeneous tectonic structures and geochemical compositions. Here we apply a transdimensional Bayesian tomography to estimate high-resolution images of group and phase velocity variations (with periods between 8 and 70 s). The method provides robust estimations of velocity maps, and the reliability of results is tested through carefully designed synthetic recovery experiments. Our maps reveal two sublithospheric low-velocity anomalies that connect back-arc regions (in Japan and Ryukyu Trench) with current margins of continental lithosphere where the volcanoes are distributed. Combined with evidences from previous geochemical and geophysical studies, we argue that the volcanoes are related to the low-velocity structures associated with back-arc processes and preexisting continental lithosphere.

1. Introduction

Northeast (NE) Asia comprises old continental lithospheres (e.g., Sino-Korean and Yangtze cratons) and their eastern margins (Figure 1), which have been extensively affected by the collision with the Indo-Australian plate and the subduction of multiple oceanic slabs (e.g., Izanagi, Kula, Pacific plate, and Philippine Sea plates) [*Ren et al*., 2002]. It has been postulated that the convergent tectonic processes have attributed the formation of rifted margins including extensional basins (Songliao, Yellow Sea, East China Sea, and Bohaiwan basins) and back-arc openings in the East Sea (Sea of Japan) and the Okinawa Trough [*Tatsumi et al*., 1990; *Ren et al*., 2002] (Figure 1a).

The Cenozoic-Recent intraplate volcanism (IPV) is widespread over NE China and the Korean Peninsula (see Figure 1). The imaged stagnant slab in the upper mantle transition zone [e.g., *Zhao and Ohtani*, 2009] defies the hot spot origin hypothesis according to which the magma sources are rooted in the lower mantle [*Tang et al*., 2014]. However, it has also been suggested that the sublithospheric mantle is the source region for alkaline basalts in the IPVs [*Choi et al*., 2006; *Kuritani et al*., 2011]. This interesting problem has provoked various interpretations for the IPV such as asthenospheric upwelling related to the oceanic slab subduction and back-arc opening [*Tatsumi et al*., 1990; *Basu et al*., 1991; *Zou et al*., 2008], geochemical and geothermal interactions between the hydrous stagnant slab and overlaying upper mantle [*Zhao and Ohtani*, 2009; *Kuritani et al*., 2011; *Wang et al*., 2015], and the leakage of a local plume through a gap in the slab [*Ai et al*., 2008; *Tang et al*., 2014; *Kim et al*., 2015]. However, posed mechanisms are difficult to reconcile with different features observed among the IPVs including scattered and long-live volcanism with low volume of magma, no evidence of spatial migration, temporal transition in magma compositions [*Zou et al*., 2008; *Zhang et al*., 2014], and heterogeneous geochemical properties [*Chung et al*., 1995; *Choi et al*., 2006]. In particular, the IPVs around the southern Korean Peninsula (e.g., Jeju, Goto, and Ulleung Islands) are different from those in NE China (e.g., Mount Baekdu or Changbai) by their different initiation time and geochemical characteristics [*Uto et al*., 2004; *Tatsumi et al*., 2005; *Choi et al*., 2006] (for the geographic locations, see Figure 1). The heterogeneity of the IPV has not been comprehensively addressed in terms of the relationship with oceanic and continental tectonic structures due to lack of evidence from geophysical imaging.

In this study, we use continuously recorded ambient noise waveform data to image seismic structures beneath NE Asia. Analyzing ambient noise dispersion data potentially increases resolution of the crust and

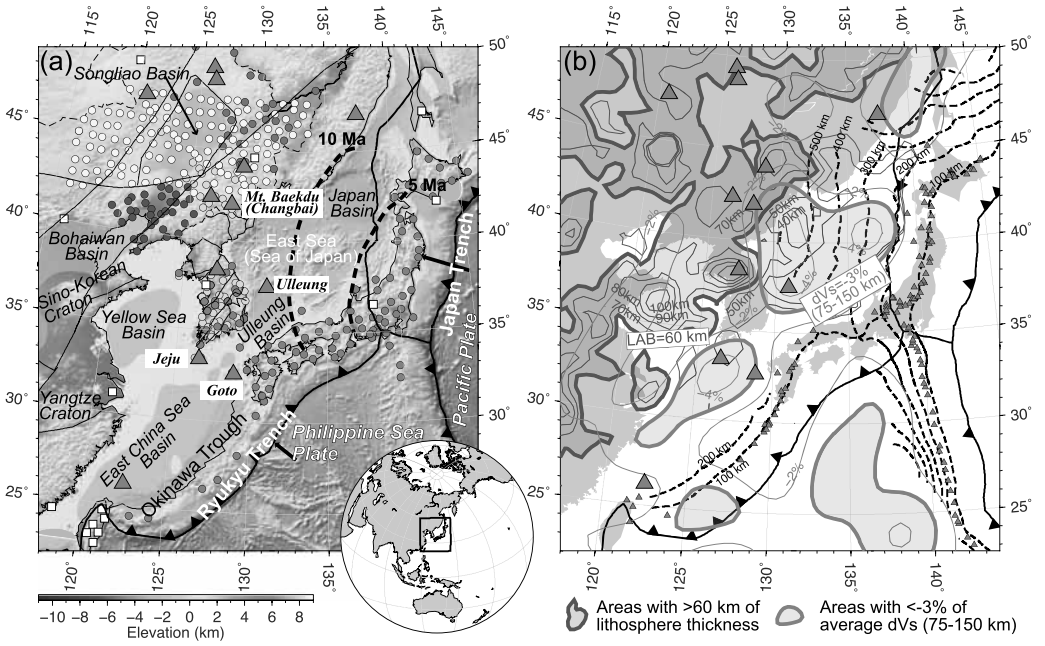

Figure 1. Maps of the region of study in NE Asia. (a) Receiver locations are shown by circles for the following networks used in this study: F-net (red), KIGAM (purple), KMA (pink), China regional arrays (blue, green, and brown), NECESSArray (yellow), and IRIS permanent stations (white squares). Elevation (color) and major sedimentary basins thicker than 1.5 km (grey) [*Laske and Masters*, 1997] are shown in the background. Locations of recent intraplate volcanoes (underlying subducting slab completely absent or deeper than 300 km) are indicated by red triangles. Reconstructed former locations of the Japan Trench [*Miller et al*., 2006] are shown by thick-dashed lines with their timings. (b) Contour map of lithosphere-asthenosphere boundary (blue lines; 10 km interval) [*Pasyanos et al*., 2014] and average shear wave velocity perturbations (red lines; 1.0% interval) to the global average in a depth range of 75–150 km [*Kustowski et al*., 2008]. The Wadati-Benioff slab interfaces are shown by contours (black dashed lines; 100 km interval). Other volcanoes along the arc/back-arc are shown by small red triangles.

shallow upper mantle due to their dominant energy at relatively shorter periods than those of earthquake-generated surface wave data. Similar imaging approaches have been applied to this region [*Zheng et al*., 2011; *Witek et al*., 2014; *Shen et al*., 2016] due to the availability of dense seismic networks. However, an uneven spatial distribution of stations mainly situated on land often results in poor resolution and inability to scrutinize tectonically important structures, such as back-arc features and magma sources beneath IPV on islands. Furthermore, the reliability of estimated model parameters is not well constrained [e.g., *Sambridge et al*., 2006], and this lack of information often results in misleading interpretations in poorly sampled regions. It is likely that the estimated uncertainties suffer from systematic bias by regularization (i.e., smoothing and damping) in many geophysical inversions (for a review, see *Rawlinson et al*. [2014]).

Here we adopt a rigorous approach to obtain high-resolution images and related uncertainties beneath NE Asia covering previously less sampled back-arc regions. We perform a type of Bayesian tomography using the transdimensional and hierarchical approach [*Bodin et al*., 2012], which has been applied to tomography studies in regional and global scales [e.g., *Young et al*., 2013a, 2013b; *Tkalčić et al*., 2015]. The method bypasses limitations typically present in an inversion by treating irregular data distribution and sensitivity through adaptive partitioning of Voronoi cells. Importantly, smearing effects and overestimation or underestimation of absolute parameter values can be avoided since the number of inversion cells and the level of data noise are implicitly balanced without the need for an explicit regularization. The key advantage of this approach is that it enables statistically meaningful estimations of resulting models and related uncertainties through a rigorous process. To demonstrate that the method recovers complex velocity anomalies within selected areas based on uncertainties, synthetic recovery tests are conducted on realistic Earth structure [e.g., *Bodin et al*., 2012; *Tkalčić et al*., 2015] that includes multiscale features and velocity gradients, and on conventional checkerboard models. In spite of uneven data sampling, high-resolution group and phase

velocity maps are obtained covering the areas of current and former back-arc regions, NE China and the Korean Peninsula. By means of dispersion velocity maps at various periods, we find evidence for a spatial relationship of the IPV and preexisting back-arc and continental structures.

2. Data and Method

Continuous broadband recordings of waveform data are retrieved from two groups of stations (Figure 1a; illustration of raypath coverage is shown in Figure S1 in the supporting information). Three years of data (2009–2011) are used for the first group (consisting of 256 stations), including a temporary array NECESSArray in NE China [e.g., *Tang et al*., 2014] and available stations in Korea, Japan, and Taiwan. To further expand ray density and coverage, we use 7 months (April–October 2014) of data including three regional networks in NE China (consisting of 218 stations).

Group and phase velocities of Rayleigh wave fundamental mode are measured for central periods of 8–70 s (see Text S1 with figures therein). To obtain interstation Rayleigh wave Green's functions, we calculate cross-correlation functions of vertical component data using the frequency-time normalization method [*Shen et al*., 2012]. From about 50,000 usable Green's functions, we measure dispersion velocities using the multiple-filter technique [e.g., *Bensen et al*., 2007]. To select high-quality data, a quality control procedure is applied based on the signal-to-noise ratio (>5) and minimum interstation distances. We remove effects of known directional sources [e.g., *Zeng and Ni*, 2010; *Zheng et al*., 2011] that potentially bias the measured velocities. To retain potentially meaningful data information, no further processes of data selection is applied. Our assessments of data quality through evaluating variations of measurements in different time intervals show consistent results. The effect of temporal variations has found to be negligible after a comparison between the two groups of broadband data for the same interstation paths.

Lateral variations of the measured group and phase velocities are estimated using the transdimensional and hierarchical Bayesian inversion method. In this method, posterior models are collected using the reversible jump Markov chain Monte Carlo technique to sample parameter space [*Bodin et al*., 2012]. To form an ensemble of the posterior models, we use 96 parallel chains and each chain progresses 300,000 iterations (approximately a maximum of 7000 CPU hours), out of which the first half is discarded to obtain converged models. The final map of each inversion is obtained by computing the arithmetic mean of samples which are represented by Voronoi cell partitioning. We assume ray theory to predict surface wave group and phase arrival times. Inconsistency introduced by the simplifying assumption is accounted for in our method through the estimated uncertainties [*Rawlinson et al*., 2014]. To account for effects of ray bending [*Bodin et al*., 2012], we iteratively update ray geometries by carrying out three preliminary inversions on 12 parallel chains and 200,000 iterations. We use uniform prior distributions of the parameters (the total number of cells, their position described by two values, the velocity value within the cells, and the level of data noise) between a minimum and maximum value obtained from the preliminary inversions (Figure S5). The prior distribution of dispersion velocities is centered on the average velocity observed at the given period with the interval of ±1 km/s.

We perform two types of recovery tests for the tomographic inversion: (a) the checkerboard test recovery and (b) the multiscale test recovery (Figure 2). To perform a checkerboard test, ±0.35 km/s and ±0.15 km/s velocity perturbations are applied to the average velocities of group and phase velocity maps, respectively. To perform the multiscale recovery test, we include the geometrical shapes in our input model that correspond to geological features observed in the region [e.g., *Zheng et al*., 2011; *Witek et al*., 2014]. Multiscale recovery test also includes several small-scale anomalies (circles with 1° diameter) and velocity gradients with perturbations of ±0.45 km/s and ±0.15 km/s for the group and phase velocities, respectively. In these tests, the Gaussian random errors are added to the travel time data. We take standard deviations of the data error distributions from the maxima of the estimated data noise parameter posterior distributions in Bayesian inversions of real data (Figure S5). In addition, the inversion results are compared to those obtained in the conventional regularized inversion method (Text S2).

3. Results and Discussion

Figures 2 and 3 show the ambient noise surface wave dispersion velocity maps from synthetic and real data tomography, respectively. Note that in these maps we "mask out" high uncertainty regions (>0.4 km/s) based on the uncertainty distributions from our real data inversions (Figure 3). The criterion for the uncertainty limit

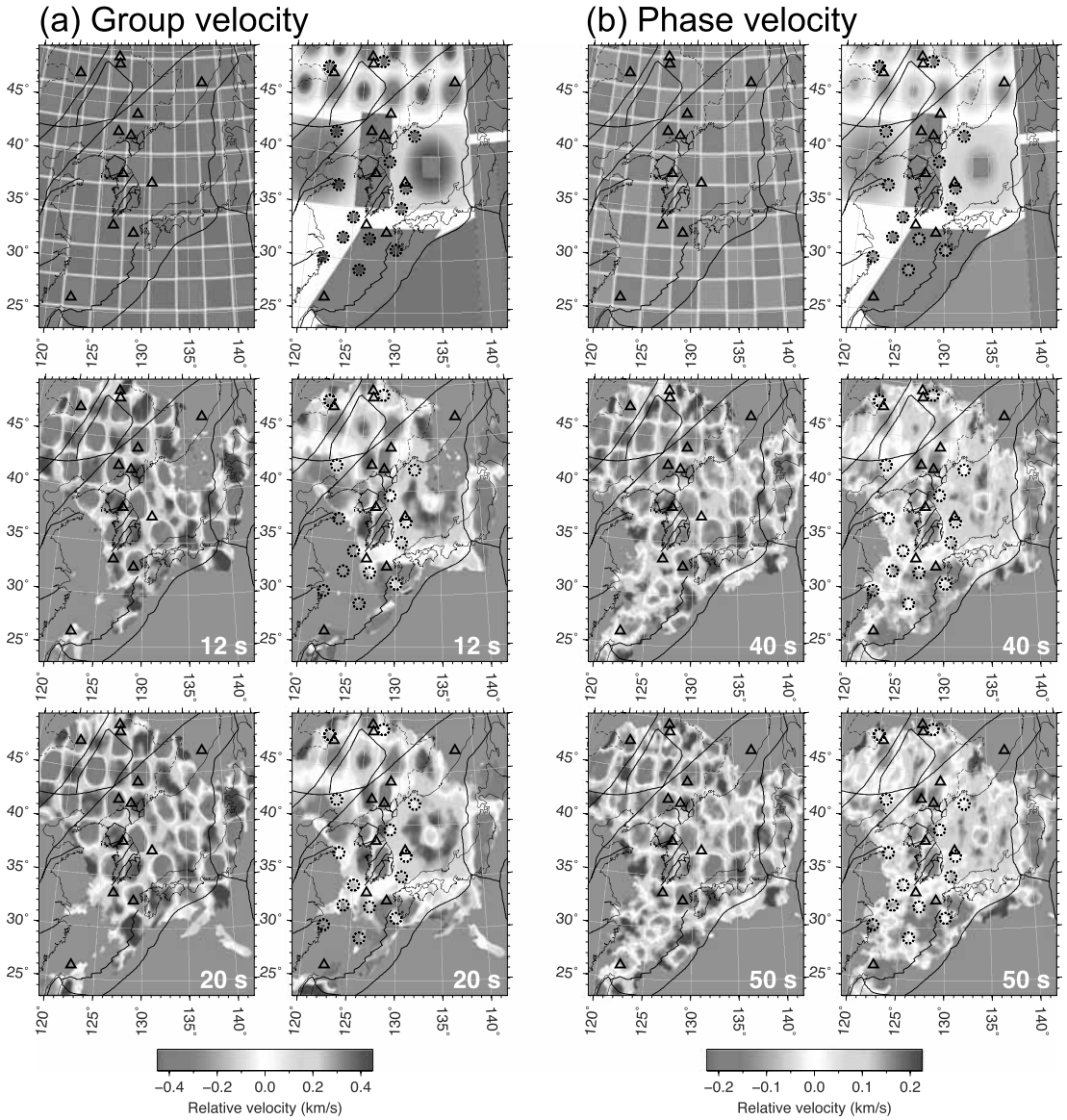

Figure 2. Results of two synthetic tests for (a) group velocity and (b) phase velocity. A checkerboard recovery is shown on the left, and a multiscale recovery is shown on the right of each pair of maps. True models used to produce synthetic data are shown in the top panel of each column. The results are shown for 12 and 20 s for the group velocity, and 40 and 50 s for the phase velocity tomography. Note that the areas of high uncertainty estimated in tomography based on the observed data (Figure 3) are masked out (gray). Solid and dashed lines indicate tectonic boundaries and slab contours (50 km interval), respectively, as shown in Figure 1. Locations of the small-scale anomalies (see the main text) are indicated by dashed circles in the true and resulting models of the multiscale recovery tests.

is empirically determined through testing residuals between the true and inverted maps from the synthetic recovery experiment (see Figure S8). In Figure 2, input velocity anomalies are well constrained including their absolute values and gradients in well-sampled regions of NE China and the Korean Peninsula. The area beneath the East China Sea basin shows relatively lower resolution due to the lower ray density (Figure S1). However, the Bayesian inversions resolve characteristic variable-scale features of the input anomalies reliably (Figure 2) compared to regularized inversions (Figure S7a), which are affected by strong smearing of input structures along the dominant raypath directions. In addition, the comparison with real data (Figures 3 and S7b) reveals that our method is highly capable in resolving complex multiscale features and sharp boundaries. Through a comparison to the inversions that utilize more refined subsets of data (Figure S9), we confirm that characteristic features in the final maps (Figure 3) are robust and consistent.

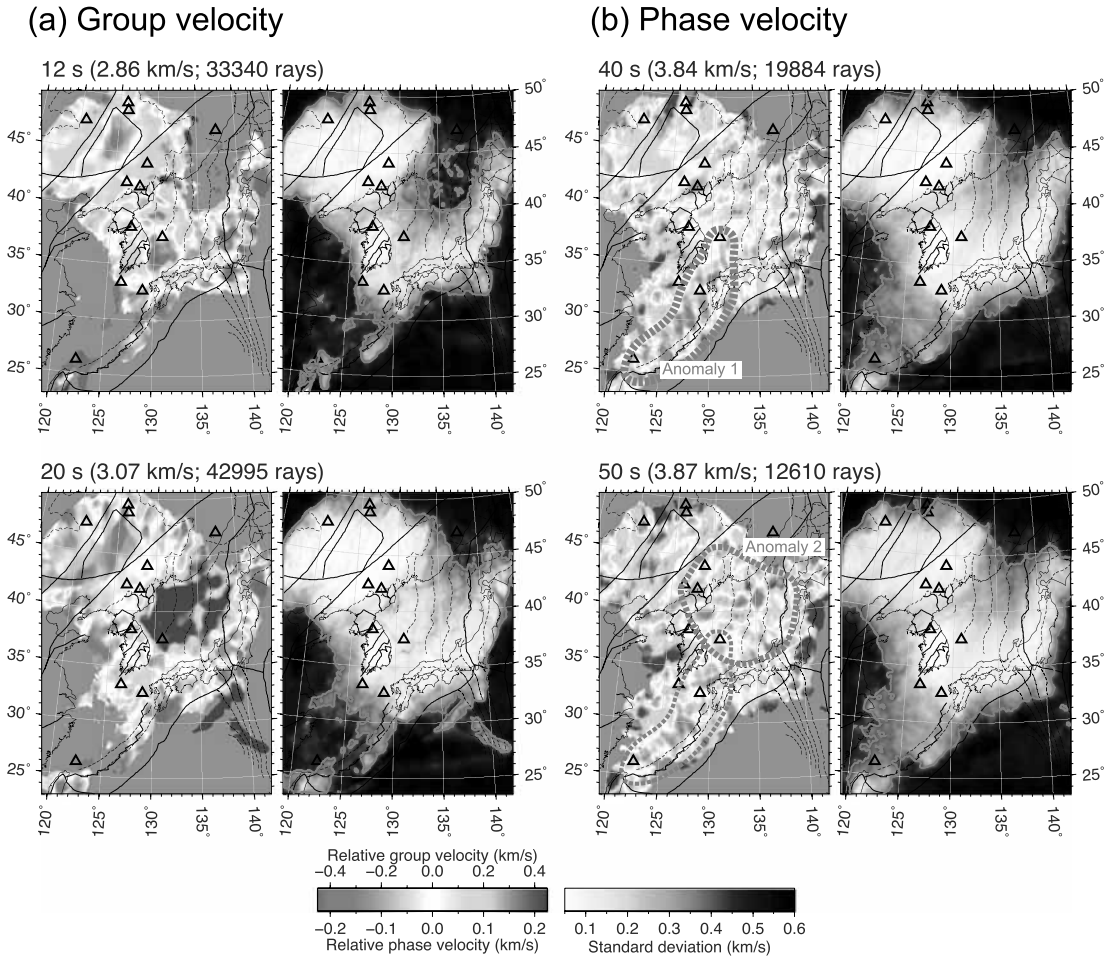

Figure 3. Dispersion velocity maps and their uncertainties for NE Asia for selected periods (indicated at the top of each map): (a) Group and (b) phase velocity. The mean velocity and the number of used data are presented in the bracket. Red isolines in each uncertainty map represent the 0.4 km/s limit used to mask out regions of high uncertainties. The areas of Anomalies 1 and 2 (see the main text) are presented by red-dashed lines in Figure 3b.

We estimate the group and phase velocity maps and their uncertainties for the period range 8–70 s with a step of 2 s (Figure 3; for other periods see Figures S10 and S11). Figure 3 shows selected maps including short (12 s) and intermediate period (20 s) for the group velocity and long period (40 and 50 s) for the phase velocity. Based on depth sensitivities of phase and group dispersion to shear wave velocity (Text S3), the presented short-period group velocity maps have a maximum sensitivity in the middle and lower crustal depths. The intermediate periods sample the upper mantle depths in significantly rifted regions, while mainly lower crust is imaged in other regions. The long-period phase velocities are predominantly sensitive to the upper mantle including the mantle lid and the top of asthenosphere beneath continental regions (lithosphere thickness $>$60 km is shown with blue contour in Figure 1b), and to the asthenospheric mantle beneath continental margin and the rifted regions.

At a period of 12 s (Figure 3a), low velocities beneath Japan likely correspond to structures associated with the dehydration process of subducting oceanic slabs [*Witek et al*., 2014]. Low-velocity anomalies in other regions show great correlation with the sedimentary structures [*Laske and Masters*, 1997] (Figure 1a), which are mainly recognized as extensional basins related to slab subductions since the Late Cretaceous [*Tatsumi et al*., 1990; *Ren et al*., 2002]. The anomaly in the East China Sea basin extends to the Jeju and Goto Islands. The Ulleung basin shows a prominent low-velocity anomaly similar to previous studies [*Witek et al*., 2014; *Lee et al*., 2015].

The sensitivity of the intermediate periods (20 s map in Figure 3a) peaks at the transitional depths between the crust and upper mantle. Strong positive velocity anomalies likely correspond to an upwelling of mantle

material beneath the East Sea and Philippine Sea, the volumes characterized by a thin rifted crust [e.g., *Zheng et al*., 2011]. We detect further details in the middle of the East Sea with relatively low velocities, which recognized as remnants of continental structures [*Ren et al*., 2002]. In addition, the high-velocity anomaly around the Jeju Island corresponds to a relatively shallow Moho depth [*Kim et al*., 2015] and thin lithosphere [*Pasyanos et al*., 2014] (Figure 1b). Low-velocity anomalies are coincidental with both the regions containing excessively thick sedimentary structures (i.e., the Songliao and Bohaiwan basins) and thick lithosphere in the central part of the Korean Peninsula and the Yellow Sea basin.

Long-period phase velocity maps (40 and 50 s; Figure 3b) show high-velocity anomalies in the central-to-southern part of the Korean Peninsula, the Yellow Sea, and NE China, corresponding to regions with relatively thick continental lithosphere (>60 km in Figure 1b). High-velocity anomalies near the Japan and Ryukyu Trenches likely present the subducting Pacific and Philippine Sea slabs, respectively. The Okinawa Trough and the East China Sea basin show strong low-velocity anomalies (Anomaly 1). Interestingly, this structure extends to IPVs in the Jeju and Goto Islands and toward the Ulleung Island (along the southern and eastern margin of the Korean Peninsula). At longer periods (50 s), low-velocity anomalies become more prominent beneath IPVs in NE China and the East Sea (Anomaly 2). The shapes of Anomalies 1 and 2 are comparable to those of surface wave dispersion velocity maps at similar periods and shear wave velocity at corresponding depths (75–150 km) estimated in previous studies [*Kustowski et al*., 2008; *Yoshizawa et al*., 2010; *Zheng et al*., 2011] (shear wave velocity perturbations are shown with red contour in Figure 1b). Strong azimuthal anisotropy potentially biases the estimated low velocities due to subparallel dominant raypath directions to the trenches (~60% in total) compared to the near perpendicular fast axis. However, relatively weak (<1%) and inhomogeneous patterns of anisotropy [e.g., *Shen et al*., 2016] compared to arc regions (e.g., ~ 2% beneath the Japanese Islands) yield a small effect near continental boundaries and IPVs in the Anomalies 1 and 2. As evidenced throughout the recovery test using multiscale anomalies, our inversions recover more complex features at these long-period maps, which have been unclear in previous studies. For instance, relatively higher velocities in the center of the East Sea correspond to regions with potentially thicker lithosphere as imaged with lower velocity at 20 s map (Figure 3a). In addition, several small-scale low-velocity anomalies coincide with locations of other IPVs in the northern part of NE China, and with a suggested tectonic boundary [*Hao et al*., 2007] along the west of the Jeju Island in the Yellow Sea.

Our images indicate the spatial transition between higher-velocity mantle lid beneath continental regions and generally lower velocity asthenospheric upper mantle beneath rifted regions. The spatial distribution of Anomaly 1 (Figure 3b) indicates that the sublithospheric low-velocity structure is confined in the area between the Ryukyu back arc and the southern edge of a thicker continental lithosphere beneath the Korean Peninsula. In association with the subduction of the Philippine Sea plate, Anomaly 1 likely captures the progression of the hot and hydrated arc and back-arc upper mantle environments, which has caused lithospheric removal, basin-forming rifting, and significant volcanism in continental margin lithosphere [*Sibuet et al*., 1987]. Anomaly 1 is described by a striking continuation to deeper depths (>75 km) in the upper mantle (Figure 1b), where the excessively low shear wave velocity (<−3% of the global average across the depth between 75 and 150 km) [*Kustowski et al*., 2008] is speculated to be a result of slab-related upper mantle upwelling [e.g., *Zhao and Ohtani*, 2009]. Consequently, our image of the anomaly depicts the pattern in greater detail at the top of this upper mantle low-velocity structure, which interacts with the relatively thick continental lithosphere. Regardless of the exact source depth [e.g., *Choi et al*., 2006; *Kuritani et al*., 2011; *Zhang et al*., 2014], it is likely that the IPVs are affected by the underlying low-velocity structure, hypothesized here to be a predominant source region for the IPVs.

We can draw similar conclusions for Anomaly 2 (Figure 3b) related to the Pacific plate subduction and IPVs in NE China: dominant low-velocity structures are confined between the eastern margin of thicker continental lithosphere beneath the NE China and Korean Peninsula, and the current back arc near the Japanese Islands. The low-velocity structure in this region corresponds to dominant back-arc extensional regions in the Ulleung and Japan basins attributed to the Japan Trench retreating since the Miocene [*Miller et al*., 2006] (Figure 1a). The scattered pattern of Anomaly 2 indicates that this process has been affected by interactions with preexisting continental lithosphere imaged as high-velocity anomalies. It is also evident that IPVs in NE China (e.g., Mount Baekdu) and near the Korean Peninsula (Ulleung) are located above the low-velocity structure. Considering previous positions of the Japan Trench (i.e., during 10–5 Ma as shown in Figure 1a), the spatiotemporal relationship between Anomaly 2 in the former back arcs and the IPVs is consistent with the current geometry of Anomaly 1.

Our images of two dominant low-velocity regions support a notion of geochemical variations in IPVs pertaining to different asthenospheric magma sources [*Choi et al*., 2006; *Chung et al*., 1995]. *Choi et al*. [2006] reported that a mixing of depleted mid-ocean ridge basalt mantle and enriched mantle (DMM-EM) 2-type magma is predominant for IPVs in southern China and the south of the Korean Peninsula compared to the DMM-EM 1 type in NE China. In concordance with the imaged features here, the generation of the DMM-EM 2-type magma might be related to Anomaly 1 by relatively incipient back arc of the Philippine Sea plate subduction. In contrast, Anomaly 2 related to the Pacific plate subduction might result in the DMM-EM 1 type rather than DMM-EM 2-type magma source. An overlap of Anomalies 1 and 2 beneath the Ulleung IPV provides explanation for the observation of intermediate compositions between the two end-members in the IPV [*Choi et al*., 2006].

We can link the IPV to the process of the oceanic slab subduction: transitions from arc/back-arc structures to intraplate environment [e.g., *Tatsumi et al*., 2000] that volcanism initiated by basal hydration in former wedge regions is maintained by slab rollback-induced decompressional melting [*Schellart and Lister*, 2005; *Zhang et al*., 2014]. The major phases of IPV are largely coeval with the timing of rollback of the slabs [e.g., *Zhang et al*., 2014; *Brenna et al*., 2015]. It has been suggested that the slab rollback of the oceanic plate plays an important role in generation of the upper mantle flow away from the arc regions [e.g., *Faccenna et al*., 2010; *Li and Niu*, 2010]. In addition, our result reveals that the recent IPVs are predominantly located near the side edge (e.g., Ulleung) and the continental margins (e.g., Jeju and Mount Baekdu) of the low-velocity anomalies as well as subducting slabs (Figure 3b). In geodynamic models, upper mantle upwelling can be displaced above slab edge due to the 3-D flow induced from rollback of slab [*Faccenna et al*., 2010; *Schellart*, 2010]. Localized edge-driven upwelling can produce IPVs [e.g., *Davies and Rawlinson*, 2014] at the margins of the Korean Peninsula and NE China where local variation of the lithospheric thickness is significant ($>$20 km) (Figure 1b) due to inherently suffered extensional basins in the East China Sea and the East Sea. In the context of the separate asthenospheric magma sources, the massive injection of asthenospheric materials from the deep upper mantle [e.g., *Kuritani et al*., 2011; *Wang et al*., 2015] can be understood as a background process [*Zhang et al*., 2014], which promotes long-lasting features of the low-velocity structures and IPVs by providing hot and hydrous upper mantle environment. The low-velocity anomalies imaged in the Bohaiwan basin and Mount Baekdu within the area of less modified continental lithosphere (Figure 3b) might be additionally affected by localized upwellings [*Ai et al*., 2008; *Kim et al*., 2015; *Tang et al*., 2014]. Nevertheless, our interpretation explains the widespread occurrence and heterogeneous features of the IPVs within the context of plate tectonics.

4. Conclusions

We obtain high-resolution group and phase velocity tomograms for NE Asia using ambient noise waveform data recorded by available permanent and temporary stations during two intervals of time: 2009–2011 and 2014. This is an extensive study that uses ~45,000 interstation paths for 32 different periods of group and phase velocity in the period range 8–70 s. The inverse problem is approached within a transdimensional and hierarchical Bayesian framework. The used method yields naturally parsimonious dispersion velocity maps, containing a balance between complexity of models and goodness of fit based on data information, while avoiding explicit parameterization. In turn, it is possible to estimate tomograms and their uncertainties avoiding arbitrary regularization and systematic biases such as smearing effects. To establish the robustness of our results, we conduct two types of synthetic recovery tests: (a) through Earth model consisting of checkerboard patterns and (b) through Earth model consisting of realistic multiscale features. The results of these tests confirm that the resolution of the imaged features is reliable within selected areas based on the estimated uncertainties. In comparison to the results from conventional, regularized inversions, the Bayesian approach is relatively void of the imaging artifacts.

The major feature that emerges from estimated dispersion velocity maps is the presence of striking low-velocity anomalies at long periods ($>$40 s). Two dominant low-velocity structures extend from current and former back-arc regions of the Philippine Sea and the Pacific plate subduction zone to the current continental margins where recently active IPVs are predominantly distributed. The pattern of low-velocity anomalies is correlated to low-velocity structures in deeper upper mantle, sedimentary basins at the surface, and relatively thinner lithosphere, which have been predominantly developed by extensional tectonic processes related to

oceanic slab subductions since the Late Mesozoic. Coupled with geochemical evidence, the extent of the sublithospheric low-velocity structures indicate that the IPVs might be affected by largely two different upper mantle source regions associated with the back-arc processes and the rollback of different subducting slabs.

Acknowledgments
The authors wish to thank two anonymous reviewers and Tae-Seob Kang for their constructive comments. This work was supported by contract FA9453-13-C-0268. J.R. was funded by the Korea Meteorological Administration Research and Development Program under grant KMIPA2015-3052. Figures presented in this paper are produced using the Generic Mapping Tool. We used data from broadband stations of the China regional networks and operated by the Korea Institute of Geoscience and Mineral Resources, the Korea Meteorological Administration, the IRIS, and the F-net. A part of inversions was performed on the Terrawulf III computational facility supported through the AuScope Australian Geophysical Observing System. AuScope is funded under the National Collaborative Research Infrastructure Strategy, and the Education Investment Fund (EIF3), both Australian Commonwealth Government Programs.

References

Ai, Y., T. Zheng, W. Xu, and Q. Li (2008), Small scale hot upwelling near the North Yellow Sea of eastern China, *Geophys. Res. Lett.*, *35*, L20305, doi:10.1029/2008GL035269.

Basu, A. R., J. W. Wang, W. K. Huang, G. H. Xie, and M. Tatsumoto (1991), Major element, REE, and Pb, Nd and Sr isotopic geochemistry of Cenozoic volcanic-rocks of Eastern China—Implications for their origin from suboceanic-type mantle reservoirs, *Earth Planet. Sci. Lett.*, *105*(1-3), 149–169.

Bensen, G. D., M. H. Ritzwoller, M. P. Barmin, A. L. Levshin, F. Lin, M. P. Moschetti, N. M. Shapiro, and Y. Yang (2007), Processing seismic ambient noise data to obtain reliable broad-band surface wave dispersion measurements, *Geophys. J. Int.*, *169*(3), 1239–1260.

Bodin, T., M. Sambridge, N. Rawlinson, and P. Arroucau (2012), Transdimensional tomography with unknown data noise, *Geophys. J. Int.*, *189*(3), 1536–1556.

Brenna, M., S. J. Cronin, G. Kereszturi, Y. K. Sohn, I. E. M. Smith, and J. Wijbrans (2015), Intraplate volcanism influenced by distal subduction tectonics at Jeju Island, Republic of Korea, *Bull. Volcanol.*, *77*(1), 1–16.

Choi, S. H., S. B. Mukasa, S.-T. Kwon, and A. V. Andronikov (2006), Sr, Nd, Pb and Hf isotopic compositions of late Cenozoic alkali basalts in South Korea: Evidence for mixing between the two dominant asthenospheric mantle domains beneath East Asia, *Chem. Geol.*, *232*(3-4), 134–151.

Chung, S. L., B. M. Jahn, S. J. Chen, T. Lee, and C. H. Chen (1995), Miocene basalts in northwestern Taiwan: Evidence for EM-type mantle sources in the continental lithosphere, *Geochim. Cosmochim. Acta*, *59*(3), 549–555.

Davies, D. R., and N. Rawlinson (2014), On the origin of recent intraplate volcanism in Australia, *Geology*, *42*(12), 1031–1034.

Faccenna, C., T. W. Becker, S. Lallemand, Y. Lagabrielle, F. Funiciello, and C. Piromallo (2010), Subduction-triggered magmatic pulses: A new class of plumes?, *Earth Planet. Sci. Lett.*, *299*(1-2), 54–68.

Hao, T. Y., Y. Xu, M. Suh, J. H. Liu, L. L. Zhang, and M. G. Dai (2007), East marginal fault of the Yellow Sea: A part of the conjunction zone between Sino-Korea and Yangtze Blocks?, *Geol. Soc. London Spec. Publ.*, *280*(1), 281–291, doi:10.1144/SP280.14.

Kim, Y., C. Lee, and S.-S. Kim (2015), Tectonics and volcanism in East Asia: Insights from geophysical observations, *J. Asian Earth Sci.*, *113*, 843–856.

Kuritani, T., E. Ohtani, and J.-I. Kimura (2011), Intensive hydration of the mantle transition zone beneath China caused by ancient slab stagnation, *Nat. Geosci.*, *4*(10), 713–716.

Kustowski, B., G. Ekstrom, and A. M. Dziewoń ski (2008), The shear-wave velocity structure in the upper mantle beneath Eurasia, *Geophys. J. Int.*, *174*(3), 978–992.

Laske, G., and G. Masters (1997), A global digital map of sediment thickness, *Eos Trans. AGU*, *78*, F483.

Lee, S.-J., J. Rhie, S. Kim, T. S. Kang, and G. B. Kim (2015), Ambient seismic noise tomography of the southern East Sea (Japan Sea) and the Korea Strait, *Geosci. J.*, *19*(4), 709–720.

Li, J., and F. Niu (2010), Seismic anisotropy and mantle flow beneath northeast China inferred from regional seismic networks, *J. Geophys. Res.*, *115*, B12327, doi:10.1029/2010JB007470.

Miller, M. S., B. L. N. Kennett, and V. G. Toy (2006), Spatial and temporal evolution of the subducting Pacific plate structure along the western Pacific margin, *J. Geophys. Res.*, *111*, B02401, doi:10.1029/2005JB003705.

Pasyanos, M. E., T. G. Masters, G. Laske, and Z. Ma (2014), LITHO1.0: An updated crust and lithospheric model of the Earth, *J. Geophys. Res. Solid Earth*, *119*, 2153–2173, doi:10.1002/2013JB010626.

Rawlinson, N., A. Fichtner, M. Sambridge, and M. K. Young (2014), Seismic tomography and the assessment of uncertainty, *Adv. Geophys.*, *55*, 1–76, doi:10.1016/bs.agph.2014.08.001.

Ren, J., K. Tamaki, S. Li, and Z. Junxia (2002), Late Mesozoic and Cenozoic rifting and its dynamic setting in Eastern China and adjacent areas, *Tectonophysics*, *344*, 175–205.

Sambridge, M., C. Beghein, F. J. Simons, and R. Snieder (2006), How do we understand and visualize uncertainty?, *Leading Edge*, *25*(5), 542–546.

Schellart, W. P. (2010), Mount Etna-Iblean volcanism caused by rollback-induced upper mantle upwelling around the Ionian slab edge: An alternative to the plume model, *Geology*, *38*(8), 691–694.

Schellart, W. P., and G. S. Lister (2005), The role of the East Asian active margin in widespread extensional and strike-slip deformation in East Asia, *J. Geol. Soc.*, *162*(6), 959–972.

Shen, W., M. H. Ritzwoller, D. Kang, Y. Kim, F.-C. Lin, J. Ning, W. Wang, Y. Zheng, and L. Zhou (2016), A seismic reference model for the crust and uppermost mantle beneath China from surface wave dispersion, *Geophys. J. Int.*, *206*(2), 954–979, doi:10.1093/gji/ggw175.

Shen, Y., Y. Ren, H. Gao, and B. Savage (2012), An improved method to extract very- broadband empirical Green's functions from ambient seismic noise, *Bull. Seismol. Soc. Am.*, *102*(4), 1872–1877.

Sibuet, J.-C., et al. (1987), Back arc extension in the Okinawa Trough, *J. Geophys. Res.*, *92*(B13), 14,041–14,063, doi:10.1029/JB092iB13p14041.

Tang, Y., M. Obayashi, F. Niu, S. P. Grand, Y. J. Chen, H. Kawakatsu, S. Tanaka, J. Ning, and J. F. Ni (2014), Changbaishan volcanism in northeast China linked to subduction-induced mantle upwelling, *Nat. Geosci.*, *7*(6), 470–475.

Tatsumi, Y., S. Maruyama, and S. Nohda (1990), Mechanism of backarc opening in the Japan Sea: Role of asthenospheric injection, *Tectonophysics*, *181*(1-4), 299–306.

Tatsumi, Y., K. Sato, T. Sano, R. Arai, and V. S. Prikhodko (2000), Transition from arc to intraplate magmatism associated with backarc rifting: Evolution of the Sikhote Alin volcanism, *Geophys. Res. Lett.*, *27*(11), 1587–1590, doi:10.1029/1999GL008436.

Tatsumi, Y., H. Shukuno, M. Yoshikawa, Q. Chang, K. Sato, and M. W. Lee (2005), The petrology and geochemistry of volcanic rocks on Jeju Island: Plume magmatism along the Asian continental margin, *J. Petrol.*, *46*(3), 523–553.

Tkalčić, H., M. Young, J. B. Muir, D. R. Davies, and M. Mattesini (2015), Strong, multi-scale heterogeneity in Earth's lowermost mantle, *Sci. Rep.*, *5*, 18,416.

Uto, K., N. Hoang, and K. Matsui (2004), Cenozoic lithospheric extension induced magmatism in Southwest Japan, *Tectonophysics*, *393*(1-4), 281–299.

Wang, X.-C., S. A. Wilde, Q.-L. Li, and Y.-N. Yang (2015), Continental flood basalts derived from the hydrous mantle transition zone, *Nat. Commun.*, *6*, 7700.

Witek, M., S. van der Lee, and T. S. Kang (2014), Rayleigh wave group velocity distributions for East Asia using ambient seismic noise, *Geophys. Res. Lett.*, *41*, 8045–8052, doi:10.1002/2014GL062016.

Yoshizawa, K., K. Miyake, and K. Yomogida (2010), 3D upper mantle structure beneath Japan and its surrounding region from inter-station dispersion measurements of surface waves, *Phys. Earth Planet. Inter.*, *183*, 4–19.

Young, M. K., N. Rawlinson, and T. Bodin (2013a), Transdimensional inversion of ambient seismic noise for 3D shear velocity structure of the Tasmanian crust, *Geophysics*, *78*(3), WB49–WB62.

Young, M. K., H. Tkalčić, T. Bodin, and M. Sambridge (2013b), Global P wave tomography of Earth's lowermost mantle from partition modeling, *J. Geophys. Res. Solid Earth*, *118*, 5467–5486, doi:10.1002/jgrb.50391.

Zeng, X., and S. Ni (2010), A persistent localized microseismic source near the Kyushu Island, Japan, *Geophys. Res. Lett.*, *37*, L24307, doi:10.1029/2010GL045774.

Zhang, M., Z. Guo, Z. Cheng, L. Zhang, and J. Liu (2014), Late Cenozoic intraplate volcanism in Changbai volcanic field, on the border of China and North Korea: Insights into deep subduction of the Pacific slab and intraplate volcanism, *J. Geol. Soc.*, *172*, 648–663.

Zhao, D., and E. Ohtani (2009), Deep slab subduction and dehydration and their geodynamic consequences: Evidence from seismology and mineral physics, *Gondwana Res.*, *16*(3-4), 401–413.

Zheng, Y., W. Shen, L. Zhou, Y. Yang, Z. Xie, and M. H. Ritzwoller (2011), Crust and uppermost mantle beneath the North China Craton, northeastern China, and the Sea of Japan from ambient noise tomography, *J. Geophys. Res.*, *116*, B12312, doi:10.1029/2011JB008637.

Zou, H., Q. Fan, and Y. Yao (2008), U-Th systematics of dispersed young volcanoes in NE China: Asthenosphere upwelling caused by piling up and upward thickening of stagnant Pacific slab, *Chem. Geol.*, *255*(1-2), 134–142.